Subwavelength far-field imaging at visible and ultraviolet wavelengths using broadband surface plasmon waves

Abdelwaheb Ourir and Mathias Fink
Institut Langevin, ESPCI, CNRS UMR 7587 Laboratoire Ondes et Acoustique, 1 rue Jussieu, 75238, Paris Cedex 05, France
(Received 30 October 2013; revised manuscript received 11 February 2014; published 5 March 2014)

The optical diffraction limit has stood for a long time in the way of achieving higher optical resolution in far-field imaging, photolithography, and optical data storage. We present here a simple and original concept for broadband far-field imaging in the visible and ultraviolet range that beats this limit. A finite-sized ultrathin metallic slab is used to encode subwavelength details of the broadband field radiated by an object. This field excites a set of surface plasmon modes on the finite-sized slab that radiates in the far field. A numerical time reversal imaging process is applied to reconstruct the image of the object with a resolution smaller than $\lambda/6$ for a gold slab and $\lambda/8$ for a silver slab. With these structures, the highest spatial frequencies are no longer limited by the pitch of the array of the subwavelength resonators as in classical metalenses. We show that the resolution depends mainly on the intrinsic properties of the metal but can be slightly controlled by the geometry design of the slab. Thanks to advances in the control of light in space and time, this concept would provide a promising alternative for high-resolution imaging techniques in the visible and ultraviolet range.

DOI: 10.1103/PhysRevB.89.115403 PACS number(s): 41.20.−q, 81.05.Xj

I. INTRODUCTION

In recent years, surface-plasmon (SP) waves have attracted a great interest because of their ability to manipulate light at a deep subwavelength scale [1–3]. Remarkable research progress and development activities, regarding SP waves, have been achieved for optical sensors detecting chemical and biological transport properties [4,5]. Surface-plasmons have been spurred by the interesting applications of strongly confined optical fields and enabled by advances in nanofabrication technology [1,2,6–8]. Self-imaging of SPs can potentially lead to challenging applications in nano-optics such as subwavelength imaging [9–12].

Usual subdiffraction imaging methods rely on scanning the surface of an object in its near field using a subwavelength probe [13–15]. Recently, high-resolution imaging through metallodielectric nanofilms have been achieved thanks to diffraction-suppressed propagation of light [16]. An important challenge lies in the coupling of conventional far-field optics to nanoscale optical circuits. Some solutions have been proposed which are based on gratings, but necessitate tedious inversion procedures [17,18]. Far-field superlenses have also been demonstrated, which are capable of magnifying evanescent waves in such a way that they become propagating [19,20]. However, these lenses show strong geometrical constraints due to the curved surfaces.

We have proposed in recent work to use a finite collection of subwavelength resonators to transmit efficiently subwavelength-scale information in the far field [21–25]. Such metalenses can convert the evanescent waves radiated by an object to propagative waves that can be collected and time reversed efficiently in the far field. Super-resolution has been experimentally achieved in microwaves [21–23] and acoustics [24], and numerically demonstrated in optics using a plasmonic metalens based on metallic nanorods [25]. This approach, based on time-reversal (TR) techniques, has been also proposed in complex-shaped nanoplasmonic systems, to impose coherent control of the spatiotemporal localization of the optical excitation energy [26,27]. Despite that this TR approach has not been experimentally demonstrated yet in optics, progresses in the spatiotemporal control of waves in the visible range should make this approach experimentally realizable soon [28–31].

One important limitation of the metalens approach, we have proposed, is that its resolution is restricted by the minimum distance between the subwavelength resonators. In this paper, we propose to replace the cluster of resonators by a finite-sized continuous medium: a finite metallic slab to overcome this limitation in optical and ultraviolet ranges. The dispersion relation of SP waves, propagating along the metallic slab interfaces, shows that high wave vectors with spatial oscillation smaller than the vacuum wavelength can be obtained. In finite-sized medium, the generated subwavelength SP modes amplified by the Fabry-Pérot-like resonances can radiate efficiently in far field. The aim of such a medium is that, theoretically, the highest spatial frequencies are no longer limited as in classical metalenses by the pitch of the array of the subwavelength resonators. Here, we demonstrate theoretically and numerically that far-field subwavelength imaging in the visible and ultraviolet ranges can be obtained with this finite medium. Nevertheless, we show that dissipation limits the imaging resolution of this approach. For instance, we show numerically that far-field subwavelength imaging can be obtained with a finite-sized gold slab in the visible range and with a silver slab in the ultraviolet range.

II. SURFACE-PLASMON RESONANT MODES

Surface-plasmon resonances strongly depend on the geometry of the structures and on the dielectric function of the surrounding medium. To obtain subwavelength SPs at visible wavelengths, we consider a slab of gold of a thickness h as shown in Fig. 1(a). For an infinite slab, the electric field propagating in vacuum above the top interface is of the form $E_z = E_0 e^{-ik_x x - \alpha z - i\omega t}$, where k_x is the propagation constant along the interface and α is the decay constant of the plasmon waves. The dispersion relation of the SPs propagating at the

 ©2014 American Physical Society

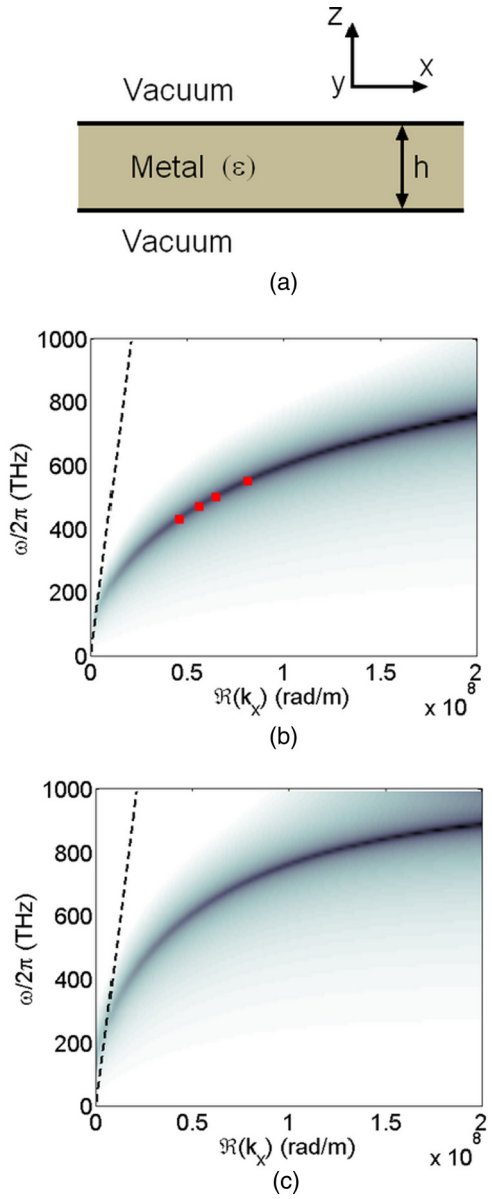

FIG. 1. (Color online) (a) Schematic view of the metallic slab surrounded by vacuum. (b) and (c) Dispersion curves for 10- and 20-nm-thick slabs, respectively. The black dotted curve is the light line, and the red dots correspond to four full wave solutions of a finite structure.

interfaces is given by the following equation [32–34]:

$$\frac{1}{\varepsilon}\sqrt{\frac{k_x^2+\varepsilon k_0^2}{k_x^2+k_0^2}} = -G\left(\sqrt{k_x^2+\varepsilon k_0^2}\frac{h}{2}\right), \qquad (1)$$

where k_0 is the wavenumber in vacuum, G is the hyperbolic tangent or cotangent function, and ε is the permittivity of the metal. Figures 1(b) and 1(c) show the dispersion curves calculated for 10- and 20-nm-thick infinite gold slabs, respectively. In both configurations, a fit of complex permittivity values taken from Ref. [35] have been considered. Only symmetric modes (according to the charge distribution), guided by the metallic slabs, are observed in the visible regime for each configuration. The asymmetric modes are at higher

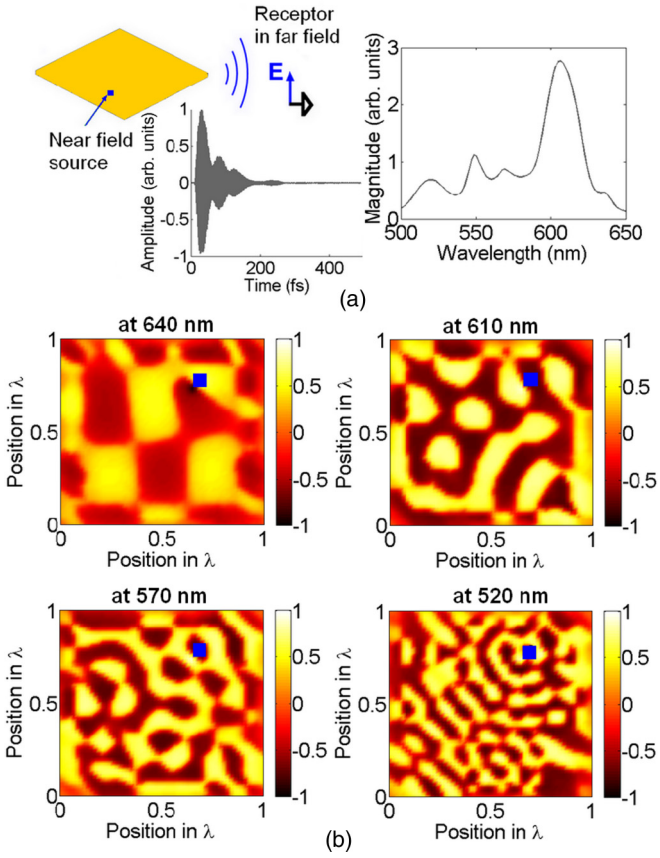

FIG. 2. (Color online) (a) Schematic view of the simulation using the finite metallic slab, time variation (left) and spectrum (right) of the calculated field radiated in far field by the small subwavelength placed over the slab. (b) Cartography of the near field normal to the interface (E_z), calculated at 10 nm over the slab for different frequencies, showing subwavelength Fabry-Pérot-like modes. The blue (dark) dot shows the position of the near-field source. We use $\lambda = 500$ nm as a reference for spatial positions.

frequencies. It can be also noted that the thinner the slab, the farther the dispersion equation is from the light line.

In the infinite-sized configuration, the electric field, propagating in vacuum above the top interface, cannot escape because the period of the field is smaller than the vacuum wavelength ($k_x > k_0$). However, in the case of a slab with a finite transverse finite size, the system behaves like a Fabry-Pérot cavity for these surface waves. To investigate this finite-sized effect, we perform finite-difference time-domain (FDTD) electromagnetic simulations (CST Software). We place a near-field source at a distance of 10 nm above the top interface of a 500-nm-large gold slab as illustrated in Fig. 2(a). We use a 4-fs-long pulse centered at 600 nm to excite the structure. With this configuration, we obtain in the far field a signal that extends over more than 300 fs [Fig. 2(a)]. This far-field signal corresponds to a wide band spectrum with many resonant peaks as it may be seen in Fig. 2(a). This spectrum results from the decomposition of the small source evanescent wave spectrum onto the SP modes of the finite slab, with a unique set of phases and amplitudes [23,22,36], that escape from the structure. Effectively, the finite size of the structure induces a wavenumber quantification. A finite

number of eigenmodes, with spatial resolution defined by the dispersion relation of the infinite medium, is generated. Because of the finite size of the structure, conversion of the subwavelength modes to propagative waves is obtained. Consequently, the generated modes can radiate efficiently with their respective patterns [22,36]. Figure 2(b) illustrates the near-electric-field maps, calculated at 10 nm above the slab, for four frequencies that correspond to four different eigenmodes of the structure. We have placed the wave vectors of these four modes on the dispersion relation plot of Fig. 1(b). As it is shown, the wave vectors of these modes are imposed by the SPs' dispersion relation of the infinite medium. This explains the "subwavelength nature" of the modes shown by the four maps of Fig. 2(b). Furthermore, the generated far-field signal [Fig. 2(a)] confirms the conversion of the subwavelength evanescent waves of the small source to propagating waves. In the proposed configuration, a variation of the field smaller than $\lambda/6$ is obtained. This resolution keeps almost constant at smaller wavelengths. Thereafter, we restrict the time-reversal process to a frequency band contained between 500 and 700 nm in the following imaging application.

III. FAR-FIELD SUBWAVELENGTH IMAGING AT VISIBLE WAVELENGTHS USING TIME REVERSAL

Some sequential steps are required in a typical time-reversal (TR) experiment. First, a short pulse is sent out from a source placed at the desired focalization location. The propagated field is then recorded with a set of receptors. Finally, the recorded signals are flipped in time and transmitted back by a set of emitters placed at the same locations of the used receptors. The application of these steps leads to a convergence of the wave to the initial source.

We propose to use the TR technique and the sketch of the imaging experiment illustrated in Fig. 3(a) to mimic a microwave metalens imaging process in the visible regime. A subwavelength object placed at a distance of 10 nm over the gold slab is illuminated with an incident plane wave. The evanescent wave spectrum, scattered by the object, decomposes onto the subwavelength modes of the slab with a unique set of phases and amplitudes. These modes radiate in the far field with good efficiency thanks to the resonant nature of the finite structure. The temporal modulation of the field resulting from the radiation of these modes is recorded on several points in the far field and, in a second step, flipped in time and back propagated numerically in a virtual system. With this process, the reconstructed image is the map of the numerically time-reversed (TR) field on the slab. The aim of this TR technique is to achieve super-resolution imaging for complex objects by using the radiated field of the subwavelength SP modes of the slab.

We start by numerically validating this technique for a punctual emitter imaging. To that aim, we perform FDTD simulations using TR techniques [37,21]. We place a number of detectors in the far field all around the metallic slab. After exciting the structure using a punctual wave source, we record the radiated field at each detector. Time-reversed waves are then generated and numerically emitted at the detector positions. Figure 3 shows the result of the imaging process. A comparison between single- and 8-detector imaging is

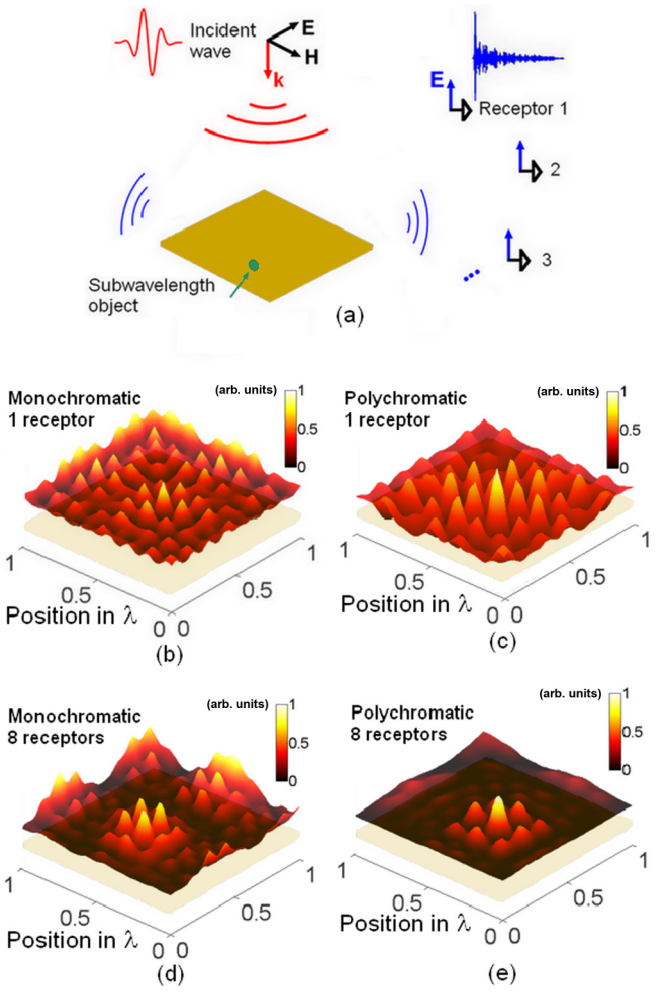

FIG. 3. (Color online) (a) Schematic view of the imaging simulation using the finite metallic slab. Focal spot obtained by (b) a monochromatic focusing at $\lambda = 520$ nm and (c) time-reversal focusing ($\lambda = 500$ to 700 nm) with only one transmitter in the far field. Focal spot obtained by (d) a monochromatic focusing at $\lambda = 520$ nm and (e) time-reversal focusing ($\lambda = 500$ to 700 nm) with eight transmitters in the far field. We use $\lambda = 500$ nm for normalizing spatial positions in all configurations.

realized in order to investigate the effect of the spatial diversity on the resolution. We have also applied this method for either monochromatic or polychromatic waves to investigate the effect of the frequency diversity. Since the modes of the structure have distinct radiation patterns, the use of 8 detectors has the advantage of collecting the maximum spatial mode signatures compared to the single-detector imaging. It reduces the side lobe level as shown in Fig. 3. Otherwise, the importance of the frequency diversity (temporal approach) is illustrated by the enhancement of the signal-to-noise ratio (SNR) obtained by the use of the polychromatic imaging. The highest SNR and resolution of $\lambda/6$ are then obtained when combining spatial and temporal diversities as shown in Fig. 3(e).

Now we image two small dipoles, emitting in the visible range, placed at a distance of 10 nm over the slab. The images obtained by time-reversal techniques for two different

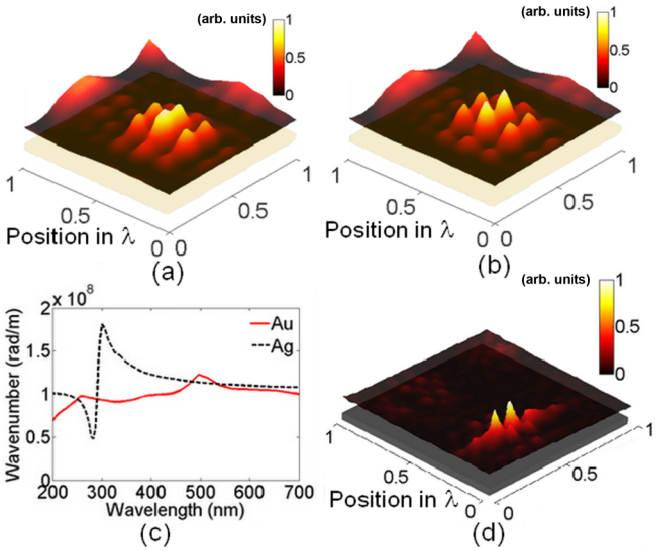

FIG. 4. (Color online) (a) Image obtained by time-reversal techniques (500 to 700 nm) of two small dipoles placed at 10 nm above the gold slab and separated by a distance of 40 nm. (b) Similar to (a), but the distance between the dipoles is 80 nm. (c) Wavenumber cutoff as a function of the wavelength. Continuous (red) line is for gold, dashed (black) line is for silver. (d) Image obtained by time-reversal techniques (320 to 420 nm) of two small dipoles placed at 10 nm above the silver slab and separated by a distance of 40 nm.

separation distances are shown in Figs. 4(a) and 4(b). As it can be seen, the resolution is about 80 nm, which is smaller than $\lambda/6$.

IV. RESOLUTION DISCUSSION: ADVANTAGE OF SUBWAVELENGTH IMAGING AT ULTRAVIOLET WAVELENGTHS

While the resolution of resonant metalenses that are composed of a cluster of resonators are limited by the lattice dimension and the losses heightened by the resonances, the resolution of this far-field lens depends only on the geometry and the intrinsic properties of the metallic slab. It is the absorption that limits the highest wave vectors $\mathbf{k_x}$ that can be radiated in the far field. Wave-vector cutoff can be evaluated just as it was shown by Podolsky *et al.* for "near-sighted" superlenses [38]. Nevertheless, we have to take account of the frequency-varying permittivity ε of the metallic slab used in our case.

Since silver presents relatively lower absorption than gold, a comparison between the imaging performances of the current gold lens and a silver lens is made in order to highlight the absorption effect. The silver lens is 350 × 350 nm of a 10-nm-thick silver slab designed to a higher frequency range. We have evaluated the wave-vector cutoff of the two far-field lenses. Figure 4(c) illustrates the variation of the wavenumber cutoff as a function of the wavelength for the two slabs. The curves show that the highest wave vectors are obtained for the wavelengths near 500 nm for the gold slab, while the highest wave vectors are around 350 nm for the silver slab. Furthermore, higher wave-vector cutoff is obtained for the silver lens thanks to its low absorption. Thereafter, we perform TR imaging for two objects placed at 10 nm above the silver slab. Figure 4(d) provides the imaging result obtained by using a polychromatic TR technique on a near-ultraviolet frequency band spread between 320 and 420 nm. A resolution of about 40 nm ($\lambda/8$) is observed. An enhancement of the resolution is obtained with this silver lens as predicted by the cutoff wave vectors presented in Fig. 4(c). Furthermore, the low absorption in the silver lens reduces the frequency-spreading width of the modes that leads to a better splitting of the modes. Thanks to this phenomenon, a higher signal-to-noise ratio in the imaging result is achieved as shown in Fig. 4(d).

Recently, it has been shown that, at sufficiently long distances, surface-plasmon polaritons (SPPs) are not the main contribution to the field. Waves similar to those existing in the radio-wave regime at the surface of the Earth, called Norton waves, are found to be stronger than SPPs at large distances [39]. While the effect of these waves, in particular on the image resolution, seems to be very weak in our case, it deserves a deeper analysis.

V. CONCLUSION

In conclusion, we have proposed to use finite-sized gold or silver slabs for subwavelength far-field imaging at visible or ultraviolet wavelengths, respectively. We have demonstrated numerically that subwavelength SPs can be excited at the interfaces of the ultrathin metallic slab and that these SPs lead to subwavelength Fabry-Pérot-like modes in the case of a finite-sized slab. By using time-reversal techniques, we have achieved far-field subwavelength imaging with these lenses. We have shown that the resolution of these lenses can be controlled by the intrinsic properties of the metal and the geometry of the slab. Compared to classical metalenses, our new approach is less sensitive to losses, and its resolution is not restricted by the minimum distance between the subwavelength resonators. Given the recent advances realized in the control of light in space and time [30,31], our concept should provide a promising alternative for classical high-resolution imaging techniques in the visible and ultraviolet range.

ACKNOWLEDGMENTS

This work is supported by LABEX WIFI (Laboratory of Excellence within the French Program "Investments for the Future") under references ANR-10-LABX-24 and ANR-10-IDEX-0001-02 PSL*.

[1] E. Ozbay, Science **311**, 189 (2006).
[2] N. Engheta, Science **317**, 1698 (2007).
[3] W. L. Barnes, A. Dereux, and T. W. Ebbesen, Nature **424**, 824 (2003).
[4] T. Zhang, H. Morgan, A. S. G. Curtis, and M. Riehle, J. Opt. A: Pure and Appl. Opt. **3**, 333 (2001).
[5] T. Chinowsky, J. Quinn, D. Bartholomew, R. Kaiser, and J. Elkind, Sensor. Actuat. B: Chem. **91**, 266 (2003).

[6] A. Polman, Science **322**, 868 (2008).
[7] T. W. Ebbesen, C. Genet, and S. I. Bozhevolnyi, Phys. Today **61**, 44 (2008).
[8] S. I. Bozhevolnyi, V. S. Volkov, E. Devaux, J.-Y. Laluet, and T. W. Ebbesen, Nature **440**, 508 (2006).
[9] L. Verslegers, P. B. Catrysse, Z. Yu, and S. Fan, Phys. Rev. Lett. **103**, 033902 (2009).
[10] G. D. Valle and S. Longhi, Opt. Lett. **35**, 673 (2010).
[11] A. G. Edelmann, S. F. Helfert, and J. Jahns, Appl. Opt. **49**, A1 (2010).
[12] M. Conforti, M. Guasoni, and C. D. Angelis, Opt. Lett. **33**, 2662 (2008).
[13] D. W. Pohl, W. Denk, and M. Lanz, Appl. Phys. Lett. **44**, 651 (1984).
[14] A. Lewis, M. Isaacson, A. Harootunian, and A. Muray, Ultramicroscopy **13**, 227 (1984).
[15] M. Burresi, D. van Oosten, T. Kampfrath, H. Schoenmaker, R. Heideman, A. Leinse, and L. Kuipers, Science **326**, 550 (2009).
[16] S. Feng and J. M. Elson, Opt. Express **14**, 216 (2006).
[17] S. Durant, Z. Liu, J. M. Steele, and X. Zhang, J. Opt. Soc. Am. B **23**, 2383 (2006).
[18] A. Sentenac, P. C. Chaumet, and K. Belkebir, Phys. Rev. Lett. **97**, 243901 (2006).
[19] Z. Jacob, L. V. Alekseyev, and E. Narimanov, Opt. Express **14**, 8247 (2006).
[20] Z. Liu, H. Lee, Y. Xiong, C. Sun, and X. Zhang, Science **315**, 1686 (2007).
[21] G. Lerosey, J. de Rosny, A. Tourin, and M. Fink, Science **315**, 1120 (2007).
[22] F. Lemoult, G. Lerosey, J. de Rosny, and M. Fink, Phys. Rev. Lett. **104**, 203901 (2010).
[23] A. Ourir, G. Lerosey, F. Lemoult, M. Fink, and J. de Rosny, Appl. Phys. Lett. **101**, 111102 (2012).
[24] F. Lemoult, M. Fink, and G. Lerosey, Phys. Rev. Lett. **107**, 064301 (2011).
[25] F. Lemoult, M. Fink, and G. Lerosey, Nat. Commun. **3**, 889 (2012).
[26] X. Li and M. I. Stockman, Phys. Rev. B **77**, 195109 (2008).
[27] M. I. Stockman, New J. Phys. **10**, 025031 (2008).
[28] J. Aulbach, B. Gjonaj, P. M. Johnson, A. P. Mosk, and A. Lagendijk, Phys. Rev. Lett. **106**, 103901 (2011).
[29] L.-C. Cheng, C.-Y. Chang, C.-Y. Lin, K.-C. Cho, W.-C. Yen, N.-S. Chang, C. Xu, C. Y. Dong, and S.-J. Chen, Opt. Express **20**, 8939 (2012).
[30] A. P. Mosk, A. Lagendijk, G. Lerosey, and M. Fink, Nat. Photonics **6**, 283 (2012).
[31] D. J. McCabe, A. Tajalli, D. R. Austin, P. Bondareff, I. A. Walmsley, S. Gigan, and B. Chatel, Nat. Commun. **2**, 447 (2001).
[32] A. A. Oliner and T. Tamir, J. Appl. Phys. **33**, 231 (1962).
[33] A. V. Zayats, I. I. Smolyaninov, and A. A. Maradudin, Phys. Rep. **408**, 131 (2005).
[34] L. Solymar and S. Shamonina, *Waves in Metamaterials* (Oxford University Press, Oxford, 2009).
[35] P. B. Johnson and R. W. Christy, Phys. Rev. B **6**, 4370 (1972).
[36] C. Jouveaud, A. Ourir, and J. Rosny, Prog. Electromagn. Res. **132**, 177 (2012).
[37] M. Fink, Phys. Today **50**, 34 (1997).
[38] V. A. Podolskiy and E. E. Narimanov, Opt. Lett. **30**, 75 (2005).
[39] A. Y. Nikitin, S. G. Rodrigo, F. J. García-Vidal, and L. Martín-Moreno, New J. Phys. **11**, 123020 (2009).